Int J Appl Earth Obs Geoinformation 68 (2018) 189–201

Contents lists available at ScienceDirect

Int J Appl Earth Obs Geoinformation

journal homepage: www.elsevier.com/locate/jag

Assessing biomass of diverse coastal marsh ecosystems using statistical and machine learning models

Yu Mo[a,*], Michael S. Kearney[a], J.C. Alexis Riter[a], Feng Zhao[b], David R. Tilley[a]

[a] Department of Environmental Science and Technology, University of Maryland, College Park, MD 20742, USA
[b] Department of Geography, University of Maryland, College Park, MD 20742, USA

ARTICLE INFO

Keyword:
Coastal marshes
Multispectral
Hyperspectral
Ground-based
Airborne
Spaceborne
Louisiana

ABSTRACT

The importance and vulnerability of coastal marshes necessitate effective ways to closely monitor them. Optical remote sensing is a powerful tool for this task, yet its application to diverse coastal marsh ecosystems consisting of different marsh types is limited. This study samples spectral and biophysical data from freshwater, intermediate, brackish, and saline marshes in Louisiana, and develops statistical and machine learning models to assess the marshes' biomass with combined ground, airborne, and spaceborne remote sensing data. It is found that linear models derived from NDVI and EVI are most favorable for assessing Leaf Area Index (LAI) using multispectral data (R^2 = 0.7 and 0.67, respectively), and the random forest models are most useful in retrieving LAI and Aboveground Green Biomass (AGB) using hyperspectral data (R^2 = 0.91 and 0.84, respectively). It is also found that marsh type and plant species significantly impact the linear model development ($P < .05$ in both cases). Sensors with coarser spatial resolution yield lower LAI values because the fine water networks are not detected and mixed into the vegetation pixels. The Landsat OLI-derived map shows the LAI of coastal mashes in Louisiana mostly ranges from 0 to 5.0, and is highest for freshwater marshes and for marshes in the Atchafalaya Bay delta. The CASI-derived maps show that LAI of saline marshes at Bay Batiste typically ranges from 0.9 to 1.5, and the AGB is mostly less than 900 g/m^2. This study provides solutions for assessing the biomass of Louisiana's coastal marshes using various optical remote sensing techniques, and highlights the impacts of the marshes' species composition on the model development and the sensors' spatial resolution on biomass mapping, thereby providing useful tools for monitoring the biomass of coastal marshes in Louisiana and diverse coastal marsh ecosystems elsewhere.

1. Introduction

Coastal marsh ecosystems offer valuable functions such as storm and flood protection, fishery resources, water purification, wildlife conservation, and carbon sequestration; yet they are increasingly under threat from natural and anthropogenic stresses including sea-level rise, hurricanes, and pollution (Morris et al., 2002; Howes et al., 2010; Deegan et al., 2012). The importance and vulnerability of coastal marshes necessitate effective ways to closely monitor them. Optical remote sensing is a powerful tool for this task. Its application for assessing coastal marshes' biomass dates back to the 1980s (Table 1). The first studies were done on *Spartina alterniflora* in saline marshes in Delaware (Hardisky et al., 1983, Gross et al., 1987). Later studies extended the application to species in lower salinity ranges to other geographic areas inside or outside the United States (Gross et al., 1986, 1993; Zhang et al., 1997; Jensen et al., 1998, 2002; Kearney et al., 2009; Trilla et al., 2013; Byrd et al., 2014; Ghosh et al., 2016). Although existing studies have demonstrated the potential of using optical remote sensing in monitoring coastal marshes at a landscape scale, they concentrated on saline marshes and focused on sites covered by single species, mostly *S. alterniflora*. How optical remote sensing can be applied to diverse coastal marsh ecosystems composed of a wide range of salinity and various plant species is less clear.

Diverse coastal marshes ecosystems, such as the ones in Louisiana, encompass habitats spanning a wide range of salinity and plant species with various leaf characteristics and canopy structures. Coastal marshes in Louisiana are subdivided into freshwater, intermediate, brackish, and saline marshes based on vegetation associations that correspond closely with the environmental modifiers such as salinity, water level, and tidal inundation duration (Gosselink, 1984; Visser et al., 2012). Plant species richness decreases from freshwater to intermediate to brackish to saline marshes, while dominance increases (Gosselink, 1984). Freshwater marshes are characterized by tall broadleaf plants (2–4 m) such as *Typha* spp., while the brackish and saline marshes are dominated by

* Corresponding author at: Department of Environmental Science and Technology, 1426 Animal Sci./Ag. Engr. Bldg., College Park, MD 20742, USA.
E-mail addresses: moyu@umd.edu, moyu6688@gmail.com (Y. Mo).

https://doi.org/10.1016/j.jag.2017.12.003
Received 13 March 2017; Received in revised form 10 December 2017; Accepted 13 December 2017

Table 1
Summary of literature using optical remote sensing to estimate coastal marsh biophysical parameters. Acronyms for **(1)** vegetation indices: normalized difference vegetation index, NDVI; infrared index, II; sample ratio, SR; soil adjusted vegetation index, SAVI; Global Environmental Monitoring Index, GEMI; atmospherically resistant vegetation index, ARVI; Soil and Atmospherically Resistant Vegetation Index, SARVI; modified chlorophyll absorption in reflectance index, MCARI; modified soil adjusted vegetation index, MSAVI; optimized soil-adjusted vegetation index, OSAVI; atmospheric and soil vegetation index, ASVI; green vegetation index, VIGreen; enhanced vegetation index, EVI; wide dynamic range vegetation index, WDRVI; chlorophyll index red, CIred; chlorophyll index green, CIgreen; infrared summation index, ISI; green normalized difference vegetation index, GNDVI; visible atmospherically resistant index, VARI; **(2)** biophysical variables: total aboveground biomass, TAB; live leaf biomass, LLB; live aboveground biomass LAB; total fresh mass, TFM; green fresh mass, GFM; aboveground green biomass, AGB; leaf area index, LAI; percent canopy cover, PCC; aboveground dead biomass, ADB; vegetation fraction, VF; leaf chlorophyll content, CHLl; and other **(3)** Partial least squares regression (PLS).

Methods	Biophysical Parameters	Best R^2	Location	Species	Reference
Landsat TM derived NDVI, II	TAB, LLB	0.9	Lewes, DE, US	*Spartina alterniflora*	Hardisky et al. (1983)
Landsat TM derived NDVI, II	TAB, LLB, LAB	0.89	Brittany, France	*Spartina anglica*	Gross et al. (1986)
Landsat TM derived NDVI	LAB,	0.7	Lewes, DE, US	*Spartina alterniflora*	Gross et al. (1987)
Landsat TM derived NDVI	LAB	0.89	Lewes, DE, US	*Typha angustifolia*	Gross et al. (1993)
Landsat TM derived SR, NDVI, SAVI, GEMI, ARVI, SARVI	TAB, TFM, GFM, AGB	0.72	San Pablo Bay, CA, US	Saline marshes	Zhang et al. (1997)
Airborne multispectral SR, NDVI, ISI, IRVIS, SAVI, ARVI, SARVI	TAB, LAI	0.77	Murrells Inlet, SC, US	*Spartina alterniflora*	Jensen et al. (1998)
Airborne multispectral SR, NDVI, SAVI	TAB, LAI	0.67	National Estuarine Research Reserve, SC, US	*Spartina alterniflora*	Jensen et al. (2002)
Landsat TM derived NDVI	LAI	0.96	Chesapeake Bay, MD, US	Brackish marshes	Kearney et al. (2009)
Narrowband MCARI, MSAVI, SR, OSAVI, NDVI	TAB, LAI	0.84	Bahia Blanca Estuary, Argentina	*Spartina alterniflora*	Trilla et al. (2013)
MODIS and Landsat derived broadband NDVI	PCC	0.82			
PLS using simulated Hyperion, Landsat 7, and World View-2	AGB	0.46	Sacramento–San Joaquin Delta, CA, US	Dominated by *Typha* spp.	Byrd et al. (2014)
PLS using image from Hyperion, Landsat 7, and World View-2	AGB	0.45			
Airborne broadband NDVI, SAVI, MSAVI, ARVI, ASVI, VIGreen with LiDAR	LAB, ADB, TAB	0.47	Galveston Island, TX, US	*Spartina alterniflora*	Kulawardhana et al. (2014)
MODIS derived broadband NDVI, EVI, WDRVI, CIred, CIgreen, SAVI, GNDVI, and VARI	LAI, VF, CHLl, AGB	0.68	Northern Gulf of Mexico, US	Saline marshes	Ghosh et al. (2016)
Landsat MSS, TM, ETM+, and OLI, ASTER, AVHRR, MODIS, SPOT, and SENTINEL-2 MSI derived SR, NDVI, ARVI, SAVI, SARVI, and EVI	LAI	0.7	LA, US	Freshwater, intermediate, brackish, and saline marshes	This study
Narrowband SR, NDVI, ARVI, SAVI, SARVI, and EVI	LAI, AGB	0.93, 0.71			
Airborne spectroscopy with random forest model	LAI, AGB	0.91, 0.84			

smaller plants that are around one-meter height or less such as *S. alterniflora* (Penfound and Hathaway, 1938).

This study examines the application of optical remote sensing on assessing biomass of the diverse coastal marsh ecosystems in Louisiana. We sample spectral and biophysical data from all freshwater, intermediate, brackish, and saline marshes, and develop statistical and machine learning models to map the biomass of the marshes with combined ground, airborne, and spaceborne data. The impacts of the species composition on the model development and the sensors' spatial resolution on biomass mapping are also investigated.

2. Methods

2.1. Ground sampling

2.1.1. Sampling sites

Forty-three sites in east Barataria Bay, LA, were sampled on 16–22 Aug 2015 (Fig. 1A; Table 2). The sites are in freshwater, intermediate, brackish, and saline marshes, corresponding to habitats with salinity of < 0.5 ppt (fresh), 0.5–5 ppt (oligohaline), 5–18 ppt (mesohaline), 18–30 ppt (polyhaline), respectively. The sites were selected because they were covered by dominant and common species in Louisiana's coastal marshes with wide ranges of canopy height and structure. Due to logistical reasons, more sites were from saline marshes compared to the other three marsh types, but the saline sites were covered by species also commonly found in the brackish, intermediate, and freshwater habitats, such as *Acnida cuspidate*, *Distichlis spicata*, *Iva frutenscens*, *Vigna luteola*, and *Spartina patens*. The sites were sampled for spectral and biophysical (i.e. leaf area index, LAI; aboveground biomass; and canopy height) data. In each site, vegetation spectral and LAI data were collected from four measurements, canopy height from three measurements, and aboveground biomass from two measurements (Fig. 1B). Average values were calculated for the multiple measurements within each site.

2.1.2. Biophysical measurements

LAI of the marshes was estimated using the GreenCropTracker software (Liu and Pattey, 2010) and downward photos taken by a camera (Canon PowerShot ELPH 110 HS, 6.16 × 4.62 mm sensor and 4 mm focal length) held at around 1.4 m height (equals to ground area about 1.5 × 2 m^2). This method derives LAI from the gap fraction of top-of-canopy digital color photography, which is strongly correlated (R^2 = 0.83) to actual LAI estimates. Briefly, this method assumes that the foliage is azimuthally uniform and spatially randomly distributed, and thus the relationship between canopy gap fraction and LAI follows the Poisson distribution. The canopy vertical gap fraction, hence, can be directly measured by quantifying the proportion of background pixels (including non-green leaf materials) of downward photos. Although this method is developed from upland crop ecosystems, it is also applicable to coastal marshes as its assumptions and calculations are not sensitive to water in the background substrates (Zhao et al., 2012).

Aboveground biomass was collected from circular plots of 0.5 m^2 (Site 1–16, 21, 22, and 25–43) or 0.26 m^2 (Site 17–20, 23, and 24). The different sizes of the plots are due to logistics reasons, but they did not impact the results because the biomass is calculated for per unit area. All aboveground biomass within the plots was gathered, put into labeled plastic bags, and then transported to the laboratory for further processing. Green (live) and brown (senescent or dead) biomass were separated. A representative subsample (around 30% by wet weight) of each sample was dried at 80 °C for 24–36 h until constant weight, weighed, and used to calculate the weight of the original sample. Aboveground green biomass (AGB), aboveground brown biomass, and

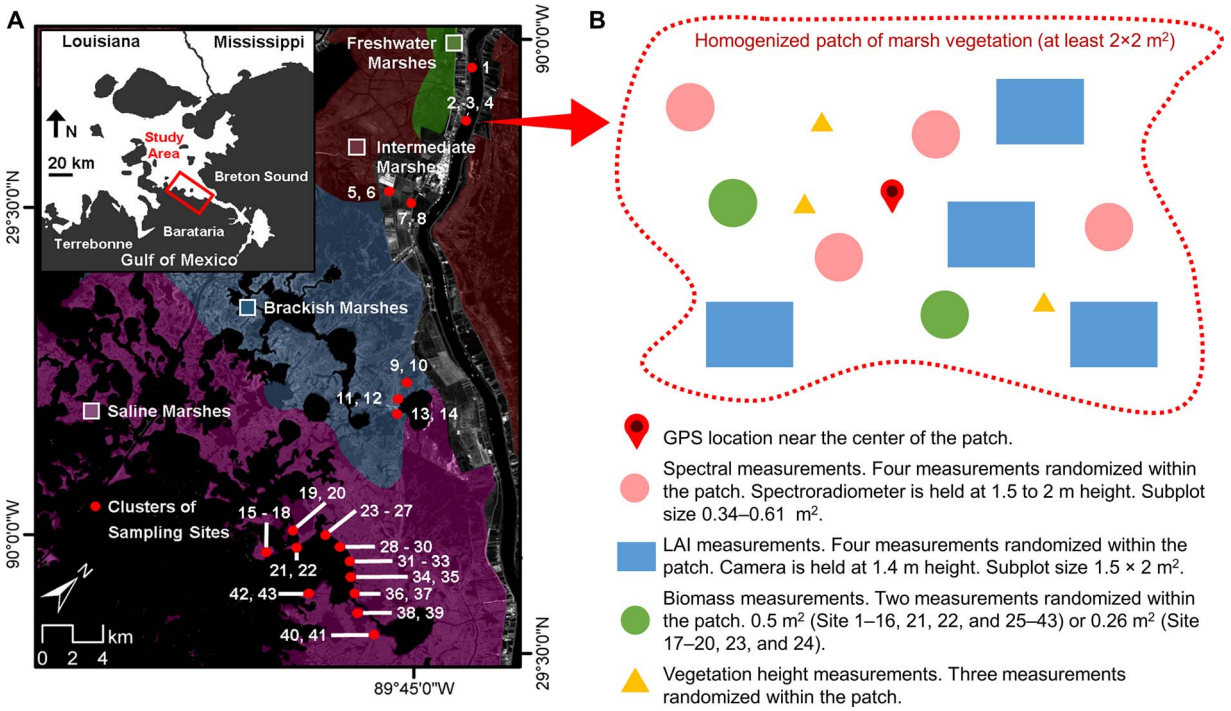

Fig. 1. Ground sampling area and design. (A) Study area in east Barataria Bay, LA. The upper left window shows the location of the study area in the context of Southeastern Louisiana. The distribution of freshwater (*green area*), intermediate (*red area*), brackish (*blue area*), and saline (*purple area*) marshes is from the U.S. Geological Survey (USGS) report in 2013. The sampling sites clusters corresponding to Table 2 are shown in *red dots*. (B) A conceptual layout of the spectral and biophysical (i.e. leaf area index, LAI; aboveground biomass; and canopy height) measurements within each site. (For interpretation of the references to colour in this figure legend, the reader is referred to the web version of this article.)

aboveground total biomass were determined by dividing the dry weight of the corresponding samples by the area of the plots (g/m^2).

2.1.3. Ground spectral measurements

Ground spectral measurements were taken by a FieldSpec 1 Spectroradiometer (ASD Inc. Boulder, CO, USA) for Site 1–14, 17–20, 23, and 24, and a FieldSpec 4 Spectroradiometer (ASD Inc. Boulder, CO, USA) for Site 15, 16, 21, 22, and 25–43. The FieldSpec 1 measures reflectance from 325 to 1075 nm and the FieldSpec 4 from 350 to 2500 nm. The spectroradiometers were set at 1.5–2-meter high with 25° field of view, corresponding to ground field of view 0.66–0.88 m and ground area of 0.34–0.61 m^2.

The ground spectral data were used to simulate spectral data of different multispectral and hyperspectral sensors to examine and compare the sensors' capability of retrieving the marshes' biomass. The spectral data of the following satellite multispectral sensors were simulated: the Advanced Spaceborne Thermal Emission and Reflection Radiometer (ASTER), the Advanced Very High Resolution Radiometer (AVHRR), the Landsat Multispectral Scanner (MSS), the Landsat Thematic Mapper (TM), the Landsat Enhanced Thematic Mapper Plus (ETM +), the Landsat Operational Land Imager (OLI), the Moderate Resolution Imaging Spectroradiometer (MODIS), the Satellite Pour l'Observation de la Terre (SPOT), and the SENTINEL-2 MultiSpectral Instrument (MSI) (Table A1). The hyperspectral data of the Compact Airborne Spectrographic Imager (CASI; 48 bands, 380–1050 nm, bandwidth 14 nm) were also simulated.

2.2. Algorithm development

2.2.1. Linear models for multispectral data

Linear models derived from broadband vegetation indices are the most common method for retrieving saline marsh biomass with multispectral sensors (Hardisky et al., 1983, Zhang et al., 1997, Ghosh et al., 2016). Following the same procedure, this study develops linear models using broadband vegetation indices calculated from simulated satellite data to assess biomass of freshwater, intermediate, brackish, and saline marshes. The broadband vegetation indices are Simple Ratio (SR), Normalized Vegetation Index (NDVI), Atmospherically Resistant Vegetation Index (ARVI), Soil-Adjusted Vegetation Index (SAVI), Soil and Atmospherically Resistant Vegetation Index (SARVI), and Enhance Vegetation Indices (EVI) (Table A2).

2.2.2. Linear models and random forest models for hyperspectral data

To evaluate the potential of hyperspectral data on assessing the marshes' biomass, this study also develops linear models using narrowband vegetation indices and full-spectrum hyperspectral data and random forest models using hyperspectral data. Linear models using narrowband vegetation indices were computed from all possible band combinations from the blue, red, and near infrared (NIR) wavelengths of the spectroradiometers. The blue wavelengths are 450–520 nm (71 bands), the red wavelengths are 580–700 nm (121 bands), and the NIR wavelengths are 700–100 nm (301 bands). For the calculation of narrowband SR, NDVI, and ARVI that only involve red and NIR bands, there are 121 × 301 = 36,421 band combinations; for narrowband EVI, SAVI, and SARVI that involve blue, red, and NIR bands, there are 121 × 301 × 71 = 2,585,891 band combinations. Linear models are also developed from simulated CASI data. As this study samples from 43 sites, we selected the first 36 bands from the blue to near infrared region from the CASI data to ensure that the number of variables in our models is less than the number of samples.

All forty-eight bands of the simulated CASI data were used to develop the random forest models. The random forest model, a non-parametric machine learning technique, constructs a number of decision trees using bootstraps (sub-samples) of the original data, and outputs the average results of the different decision trees. There are two layers of randomness in the random forest model: (1) each decision tree is constructed using a random bootstrap; and (2) each node is split using a random subset of predictors. The two layers of randomness

Table 2
Sampling site descriptions. Sites are from four marsh types: freshwater (F), intermediate (I), brackish (B), and saline (S) marshes. When listed for the first time, a species is followed by its wetland indicator status: obligate (OBL), facultative wetland (FACW), facultative (FAC), facultative upland (FACU). In sites have more than one species, the numbers following the species names show their percent coverage (%).

Site	Center Coordinates (latitude, longitude)	Type	Species
1	29.754823 -90.036592	F	*Spartina spatinae* (OBL)
2	29.701181 -89.989879	F	*Paspalum dissectum* (OBL)
3	29.700944 -89.989924	F	*Setaria glauca* (FAC)
4	29.700907 -89.988767	F	*Spartina cynosuroides* (OBL, 70); *P. dissectum* (30)
5	29.662671 -90.994669	I	*Zizaniopsis miliacea* (OBL)
6	29.662405 -89.995485	I	*Sesbania macrocarpa* (FACW-, 70); Aster spp. (30)
7	29.663415 -89.991279	I	*Z. miliacea*
8	29.661961 -89.995635	I	*Panicum repens* (FACW-)
9	29.574779 -89.901653	B	*Distichlis spicata* (FACW+, 50); *Vigna luteola* (FACW, 50); *Lythrum lineare* (2, OBL)
10	29.574737 -89.901490	B	*Iva frutenscens* (FACW+, 50); *D. spicata* (50); *V. luteola* (2)
11	29.567115 -89.891173	B	*S. cynosuroides* (90); *Spartina patens* (FACW, 10)
12	29.567204 -89.891221	B	*S. patens* (95); *D. spicata* (5); *L. lineare* (2)
13	29.563997 -89.888460	B	*S. cynosuroides* (90); *D. spicata* (5); *Ipomoea sagittata* (FACW, 5); *Scripus americanus* (OBL, 2); *Acnida cuspidate* (OBL, 2)
14	29.564025 -89.888804	B	*S. patens* (90); *D. spicata* (10)
15	29.438646 -89.875689	S	*Batis maritima* (OBL)
16	29.438450 -89.876186	S	*D. spicata* (90); *B. maritima* (10)
17	29.456000 -89.876550	S	*Juncus roemerianus* (OBL)
18	29.446137 -89.876094	S	*Spartina alterniflora* (OBL)
19	29.461626 -89.875924	S	*J. roemerianus* (90); *S. alterniflora* (10)
20	29.461700 -89.874700	S	*S. alterniflora*
21	29.455363 -89.864686	S	*S. alterniflora*
22	29.455316 -89.864683	S	*V. luteola* (80); *J. roemerianus* (10); *S. alterniflora* (10)
23	29.475133 -89.856300	S	*J. roemerianus*
24	29.474251 -89.856777	S	*S. alterniflora*
25	29.473703 -89.859188	S	*A. cuspidata* (80); *D. spicata* (20); *I. frutenscens* (10)
26	29.473362 -89.858871	S	*Borrichia frutescens* (OBL, 50); *D. spicata* (50)
27	29.473474 -89.859623	S	*D. spicata*
28	29.476477 -89.849812	S	*S. alterniflora*
29	29.476409 -89.849805	S	*S. patens*
30	29.476193 -89.839526	S	*B. frutescens* (80); *S. patens* (20)
31	29.467183 -89.839433	S	*S. patens* (90); *I. sagittata* (10)
32	29.473750 -89.833250	S	*S. alterniflora*
33	29.473632 -89.833144	S	*S. patens* (95); *S. alterniflora* (5)
34	29.466026 -89.823338	S	*A. cuspidata* (30); *S. alterniflora* (30); *B. maritima* (20); *I. frutenscens* (20)
35	29.465913 -89.823340	S	*B. maritima* (60); *S. patens* (40)
36	29.460335 -89.815582	S	*J. roemerianus*
37	29.460261 -89.815555	S	*S. alterniflora*
38	29.455847 -89.802297	S	*J. roemerianus*
39	29.456057 -89.802120	S	*S. alterniflora*
40	29.451356 -89.784136	S	*J. roemerianus* (90); *S. alterniflora* (10)
41	29.451396 -89.784172	S	*S. alterniflora*
42	29.442733 -89.834981	S	*A. cuspidata* (50); *S. alterniflora* (50)
43	29.442803 -89.834923	S	*D. spicata*

Table 3
Descriptive statistics of the biophysical measurements of the study sites (n = 43).

Variable	Mean	Standard Deviation	Min	Max
Aboveground green biomass (g/m^2)	630	328	121	1428
Aboveground brown biomass (g/m^2)	664	564	10	2643
Total aboveground biomass (g/m^2)	1263	714	369	3472
Canopy height (cm)	104	50	32	224
LAI	2.48	1.20	0.50	4.89

improve prediction accuracy and control over-fitting (Liaw and Wiener, 2002; Cutler et al., 2007).

2.3. Mapping the marshes biomass using airborne and spaceborne data

We estimated LAI of the coastal marshes in Louisiana using Landsat data with the linear models developed in this study. The LAI of the entire coastal marsh ecosystem in Louisiana was mapped using eight scenes from the Landsat Surface Reflectance Climatic Data Record that were collected during the summer in 2015 (Table A3).

LAI and AGB maps of marshes near Bay Batiste in east Barataria Bay were produced using CASI data and the random forest model developed in this study. The CASI data were collected on August 16, 2015, with flight altitude of 2400 m. The data were collected in spatial resolution of 1.2 m and with 48 bands (bandwidth 14.4 nm) at 380–1050 nm.

To study the impacts of spatial resolution of the sensors on biomass assessment, we compared the LAI maps of saline marshes near Bay Batiste generated from CASI data, Landsat OLI data, and MODIS data (with spatial resolution of 1.2 m, 30 m, and 250 m, respectively). The MODIS data was the MODIS13Q1 Terra Vegetation Indices 16-day composite (250 m) acquired from August 13–28 2015. The CASI-map was downscaled into two maps with spatial resolution of 30 m and 250 m and the Landsat-map into one map with spatial resolution of 250 m.

2.4. Software

The field spectral data was processed using ViewSpec Pro 6.2 (ASD Inc., Boulder, CO, USA), and the airborne and satellite data using ArcGIS 10.1 (Esri Inc., Redlands, CA, USA) and ENVI 5.0 (Exelis Visual Information Solutions, Boulder, CO, USA). The development of linear models and the random forest models was performed in R 3.2. The impacts of sensor spectral characteristics, marsh types, and species on the linear models were tested using Analysis of covariance (ANCOVA) in SAS 9.3 (SAS Institute, Cary, NC, USA).

Table 4
Linear models developed from broadband vegetation indices (BVI; i.e. simple ratio, SR; normalized vegetation index, NDVI; Atmospherically Resistant Vegetation Index, ARVI; Soil-Adjusted Vegetation Index, SAVI; Soil and Atmospherically Resistant Vegetation Index, SARVI; and Enhance Vegetation Indices, EVI) using simulated spectral information of Landsat Multispectral Scanner (MSS) and other sensors (i.e. Advanced Spaceborne Thermal Emission and Reflection Radiometer, ASTER; Advanced Very High Resolution Radiometer, AVHRR; Landsat Thematic Mapper, TM; Landsat Enhanced Thematic Mapper Plus, ETM+; Landsat Operational Land Imager, OLI; Moderate Resolution Imaging Spectroradiometer, MODIS; Satellite Pour l'Observation de la Terre, SPOT; and SENTINEL-2 MultiSpectral Instrument, MSI), and from narrowband vegetation indices (NVI). ([a] Narrowband vegetation indices calculated from optimal wavelength regions. The optimal wavelength regions are shown in Figs. A2 and A3.)

BVI for Landsat MSS		BVI for other sensors and NVI		
Linear Models	R^2	Linear Models	R^2 (BVI)	R^2 (NVI[a])
LAI = 5.14700–11.95650 × SR	0.71	LAI = 4.86335 −15.23824 × SR	0.69	> 0.72
LAI = −3.42725 + 9.17524 × NDVI	0.72	LAI = − 5.17840 + 10.40845 × NDVI	0.70	> 0.72
LAI = −0.36579 + 7.01687 × SAVI	0.70	LAI = − 0.82688 + 6.36472 × SAVI	0.68	> 0.72
–	–	LAI = − 0.04168 + 4.28377 × EVI	0.67	> 0.69
–	–	LAI = − 2.35296 + 7.25352 × ARVI	0.71	> 0.74
–	–	LAI = − 0.39733 + 5.91271 × SARVI	0.72	> 0.69

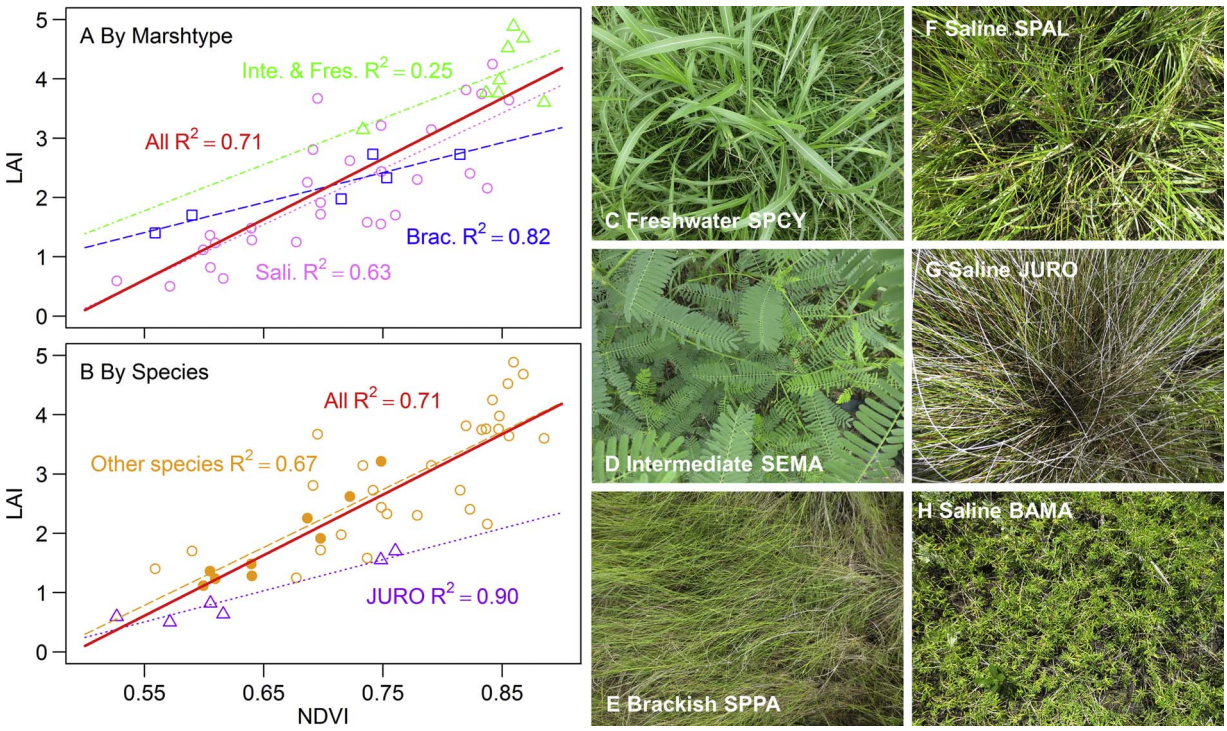

Fig. 2. Linear models for assess the marshes LAI using simulated Landsat TM NDVI: (A) by marsh type, freshwater and intermediate (*green triangles*), brackish (*blue squares*), and saline marshes (*pink cycles*); and (B) by Species, *Juncus roemerianus* (*purple triangles*), *Spartina alterniflora* (*filled orange cycles*), and the other species (*open orange cycles*). The linear model developed using all the data points are shown in *red*. (C)-(H) Downward photographs of *Spartina cynosuroides* in a freshwater mashes site, *Sesbania macrocarpa* in an intermediate marshes site, *Spartina patens* in brackish marshes, and *Spartina alterniflora*, *Juncus roemerianus*, and *Batis maritima* in saline marshes sites, respectively. (For interpretation of the references to colour in this figure legend, the reader is referred to the web version of this article.)

3. Results

3.1. Vegetation in the ground sampling sites

The sampling sites are covered by dominant and common species in Louisiana's coastal marshes, such as *Zizaniopsis miliacea* and *Paspalum dissectum* in freshwater and intermediate marshes, *Spartina patens* and *Distichlis spicata* in the brackish marshes, and *S. alterniflora*, *Juncus roemerianus*, and *Batis maritima* in the saline marshes (Table 2) (Penfound and Hathaway, 1938; Chabreck, 1972; Visser et al., 1998). It should be noted that many of these species are common in different marsh types, but their order of dominance changes. As our study sites were covered by various species that have distinct canopy structures, they show broad ranges of AGB, aboveground brown biomass, total aboveground biomass, canopy height, and LAI (Table 3). The AGB ranges from 121 to 1428 g/m^2, the canopy height from 32 to 244 cm, and the LAI from 0.5 to 4.89. Different species show different spectra, especially at the NIR region from 900 to 1200 nm (Fig. A1). We argue that the divergent vegetation conditions in our sites are representative for the entire coastal marshes ecosystem in Louisiana and diverse marsh ecosystems elsewhere.

3.2. Linear models for multispectral data

The linear models derived from broadband vegetation indices using simulated satellite data provide strong predictions for LAI of the marshes (R^2 = 0.66–0.69; Table 4). The correlation between the broadband vegetation indices with the AGB, aboveground brown biomass, total biomass, and vegetation height were poor (R^2 < 0.1, data not shown). The similar performances of the different indices may be due to the fact that, although the indices use different coefficients to increase their sensitivity and correlation, they all based on normalizing the difference between red and NIR bands (Ghosh et al., 2016). The models using simulated Landsat MSS data are significantly different from models

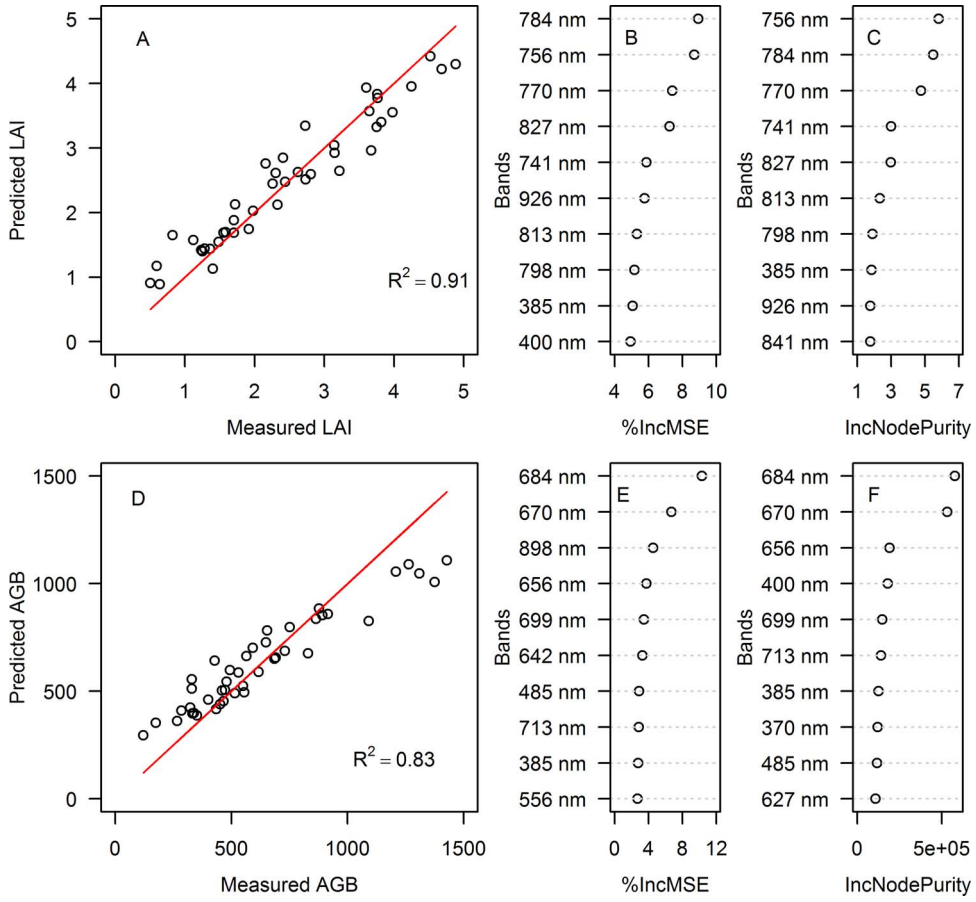

Fig. 3. Correlation between the measured leaf area index (LAI) and aboveground green biomass (AGB) and their predicted values from random forest model (A and D), and the ten most important bands for the predictions in terms of increasing mean squared error (MSE) and node purity for the predictions of LAI and AGB (B, C, E, and F, respectively).

using simulated data of other sensors (i.e. ASTER, AVHRR, Landsat TM, Landsat ETM+, Landsat OLI, MODIS, SPOT, and SENTINEL-2 MSI; $P < 0.05$). This result likely reflects the distinct NIR band of Landsat MSS which is closer to the red light wavelengths compared to the those of other sensors.

Our results indicate that the linear models derived from NDVI and EVI, with their own advantages and disadvantages, are most useful for assessing the marshes biomass for long term studies at the regional scale. NDVI shows the strongest correlation with the marshes studied LAI ($R^2 = 0.7$). Moreover, with a simple formula only requiring information from the red and near infrared band. It thus can be calculated from data of most satellite-based multispectral sensors including the Landsat MSS that provides data goes back to 1970s. NDVI, nevertheless, tends to underestimate biomass of marshes in areas with sparse or low vegetation. For example, LAI of marshes along the shoreline, where NDVI is less than 0.5 but more than zero, is zero. On the other hand, EVI, despite its slightly lower R^2 of 0.67, gives better LAI estimation of marshes in areas with low vegetation, probably because the soil adjustment factor in the EVI formula balances out the background signals from soil and water underneath the marshes. However, as EVI requires spectral information from the blue light wavelength, it can only provide data of the marshes since 1984 (with Landsat TM); this is 10 years less than the NDVI data.

The impacts of marsh type and species composition on the linear model development were tested using simulated Landsat TM NDVI (Fig. 2). The freshwater and intermediate marshes are combined due to the limited sampling sites in two marsh types. Results show that the linear models are significantly different for different marsh types, i.e., freshwater and intermediate, brackish, and saline marshes ($p < .05$, Fig. 2A). As several of our sites were mostly covered by of *J. roemerianus* and *S. alterniflora* (six and nine sites, respectively), we compared the linear models for *J. roemerianus*, *S. alterniflora*, and all the other species. The linear model derived for *J. roemerianus* is significantly different from the model for the other species ($p < .05$), but the model for *S. alterniflora* is not (Fig. 2B).

Our results suggest that LAI is a better biophysical parameter to be retrieved by multispectral remote sensing for marshes coastwide regardless of species composition. LAI strongly relates with canopy photosynthesis and dry matter accumulation in situations where stress (water, disease, pests, etc.) does not predominate as LAI's magnitude and duration are related strongly to the canopy's ability to intercept photosynthetically active radiation (Asrar et al., 1985). Moreover, direct measurements of LAI are labor intensive and not feasible for regional studies. Hence the development of a non-destructive, simple, and rapid technique for assessing leaf area is an important contribution for large-scale coastal marsh studies.

3.3. Linear models and random forest models for hyperspectral data

The linear models derived from the narrowband vegetation indices provide strong predictions for LAI ($R^2 > 0.74$ for ARVI, Table 4) but not for AGB ($R^2 > 0.25$, data not shown). The linear models derived from the simulated CASI data (band 380–855 nm) shows strong predictive capabilities for both LAI and AGB ($R^2 = 0.93$ and 0.71, respectively). There are 27 and 30 variables/bands selected for the final models for LAI and AGB through stepwise regression (Table A4). The random forest models derived from the simulated CASI data also provide strong predictions for both LAI and AGB ($R^2 = 0.91$ and 0.84, respectively; Fig. 3). The most important variables for predicting LAI are NIR bands at 784 and 756 nm (Fig. 3B and C), and for predicting

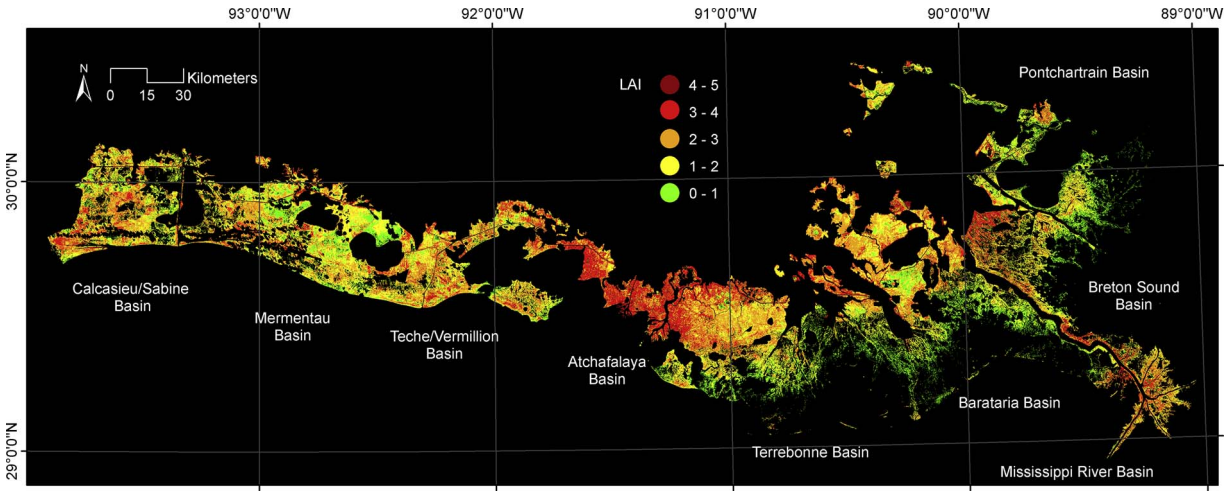

Fig. 4. Leaf area index (LAI) of coastal marshes in Louisiana derided from Landsat OLI imagery collected in 2015 summer.

ABG are red bands at 684 and 670 nm (Fig. 3E and F). However, due to the potential multicollinearity among reflectance of the bands, the conclusions drawing on the importance of the bands for the linear models and the random forest models are only applicable to the datasets used in this study. The results of this study suggest that if hyperspectral spectra are available, the random forest models are preferable as they yield high R^2 for both LAI and AGB. The better performance of the random forest model may be due to that they fully utilize the full-spectrum hyperspectral data, and make no assumption of the approximate normality of the sampling population.

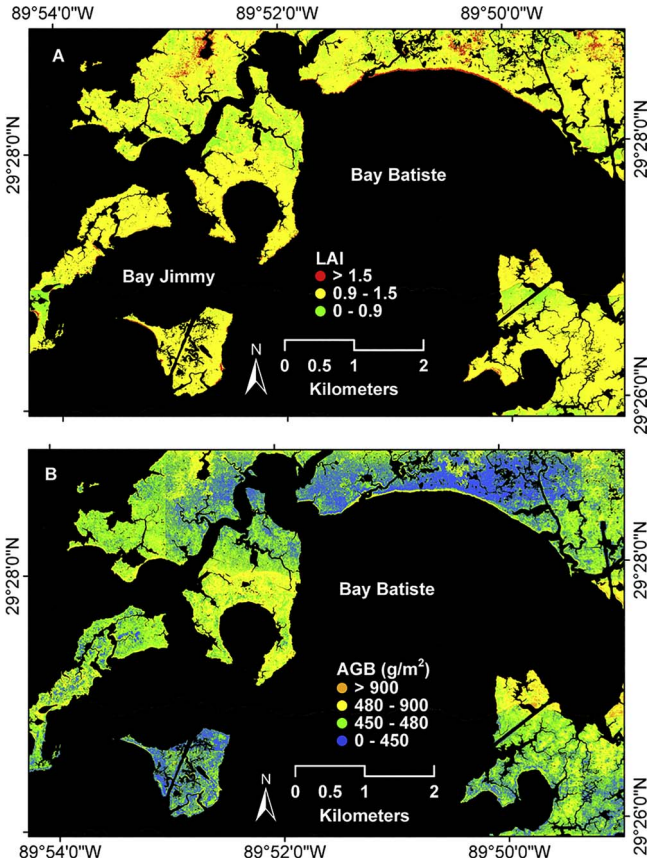

Fig. 5. Leaf area index (LAI) (A) and aboveground green biomass (AGB) (B) of coastal marshes near Bay Batiste in east Barataria Bay derived from CASI hyperspectral data collected in August 16, 2015.

3.4. Biomass mapping using CASI and Landsat

LAI of coastal marshes in Louisiana was mapped using Landsat OLI imagery collected in summer of 2015 and employing a linear model developed in Section 3.2 (i.e. LAI = − 0.04168 + 4.28377 × EVI) (Fig. 4). The LAI ranges from 0 to 5.0; and is highest for freshwater marshes (> 1.0) and for marshes in the Atchafalaya Bay delta (> 2.0). LAI and ABG of marshes near Bay Batiste were mapped using the CASI hyperspectral data and the random forest models developed in Section 3.3 (Fig. 5). The LAI in the area typically ranges from 0.9 to 1.5, and the AGB is mostly below 900 g/m^2. The results generally agree with previous field studies (Hopkinson et al., 1978, Visser et al., 2006).

Fig. 6 compares the LAI maps of saline marshes near Bay Batiste in east Barataria Bay derived from CASI, Landsat, and MODIS data. The data on pixels in the upper left corner of the Landsat map are missing due to cloud coverage. The amount and detail of the tidal creek/water network reduce and the estimated LAI decreases from the CASI map to the Landsat map to the MODIS map (Fig. 6A, D, and F, respectively). The same phenomenon occurs when we downscaled the CASI map from 1.2 m spatial resolution to 30 m and 250 m (Fig. 6A–C), and the Landsat map from 30 m spatial resolution to 250 m (Fig. 6D and E).

4. Discussion

4.1. The impacts of species composition on model development

We find that species composition of the sampling sites significantly impacts the model development. This result is not surprising as the zonation of coastal marshes is well established (Penfound and Hathaway, 1938; Chabreck, 1972; Visser et al., 1998). Freshwater and intermediate mashes are characterized by tall broadleaf species, such as *Spartina cynosuroides* and *Sesbania macrocarpa* shown in Fig. 2C and D, respectively. Saline marshes have mostly smaller plants that are around one-meter height or less, such as *S. alterniflora*, *J. roemerianus*, and *Batis maritima* shown in Fig. 2F–H, respectively. This study also finds that the linear model for *J. roemerianus* is significantly different from the model for the other species. The reasons for this result are not fully clear, but may be related to the erectophile canopy and the dark color of *J. roemerianus* (Fig. 2G). Although soil background and water levels may impact the linear models for assessing the marshes biomass (Huete, 1988; Kearney et al., 2009), we tried to minimize such influences by sampling sites at similar conditions (at low water level and dark organic soil). The results suggest that previous models developed based on saline marshes and certain species need to be revised before being applied to diverse coastal marshes ecosystems comprising other marsh types, i.e. brackish, intermediate, and freshwater marshes.

4.2. The impacts of the spatial resolution of sensors on biomass mapping

It is shown that maps with larger pixel size show less water network and yields lower LAI values for the same area. This holds both for maps generated from sensors with coarse spatial resolutions, and for maps that downscaled from higher-spatial-resolution maps. Previous studies suggested the "averaging effect" of spectral signals of different plant species in large pixels (Ghosh et al., 2016). This study further argues that the "averaging effect" also exists in signals from vegetation and non-vegetation areas. Coastal marshes are highly heterogeneous environments consisting of vegetation, bare soil, and water. Maps with larger pixels are not able to detect fine water networks and small areas of bare soil, which are then mixed into the vegetation pixels and "dilute" the vegetation signals. This phenomenon is not about the accuracy in assessing the marshes' LAI: The same area can be represented by one MODIS 250 × 250 m^2 pixel with median LAI, or by several 30 × 30 m^2 Landsat pixels with a mix of high-LAI-vegetation pixels and water pixels. Yet, the "averaging effect" could lead to loss of the marsh vegetation information in areas with high coverage of water. For example, the vegetation pixels along the shorelines in CASI and Landsat data were idenfied as water pixels in the MODIS data (Fig. 6C, E, and F). Therefore, sensors with high spatial resolution are preferred for mapping the areas with dense water networks and areas along shorelines.

4.3. Biomass of coastal marshes in Louisiana

Results from this study generally agree with previous field studies measuring the marshes' biomass (Hopkinson et al., 1978; Visser et al., 2006). The MODIS derived-LAI in the study area (0– above 2.5) from a previous study is lower than the Landsat derived-LAI (0–5) from this study (Ghosh et al., 2016), which is likely due to the averaging of vegetation and background signals of the large MODIS pixels as discussed in Section 4.2. LAIs were highest for freshwater marshes and lowest for saline marshes, which is expected since freshwater marshes generally are characterized by high primary production owing to high nutrient subsidy and low stress from saline soils (Good et al., 1978; Waide et al., 1999). Higher LAI is observed in the Atchafalaya Bay delta. This also meets our expectation as the Atchafalaya Bay delta is in the active-growing stage of its delta life cycle and receives more riverine sediment and surface runoff with high nutrients (Gosselink, 1984). The Mississippi River Delta is the other delta in Louisiana in its active-growing stage, but its LAI was not as high as the Atchafalaya Bay Delta. This is perhaps because the Mississippi River Delta has more water networks such canals, therefore its vegetation reflectance signals were not as strong as the ones from the Atchafalaya Bay Delta.

The R^2 values of the linear models generated in this study are lower, although still comparable, with previous work (Table 1), which is likely due to heterogeneity of the sampling sites in this study. The R^2 values of the random forest models are among the best results. It should be noted that as the R^2 values in this study are based on simulated spectral data, they are comparable to results also obtained from simulated spectral data (Hardisky et al., 1983; Gross et al., 1986, 1987; Zhang et al., 1997; Byrd et al., 2014), but may be somewhat optimistic when compared to results directly correlating ground measurements and satellite observations (Byrd et al., 2014; Ghosh et al., 2016). As samples patches with homogenous vegetation with no fixed size, we are not able to provide ground true for sensors at specific spatial resolutions. Nevertheless, our sampling site cover all coastal freshwater, intermediate, brackish, and saline marshes, they, thus, better represents species diversity of coastal marshes, thereby contributing to biomass mapping of diverse coastal marsh ecosystems.

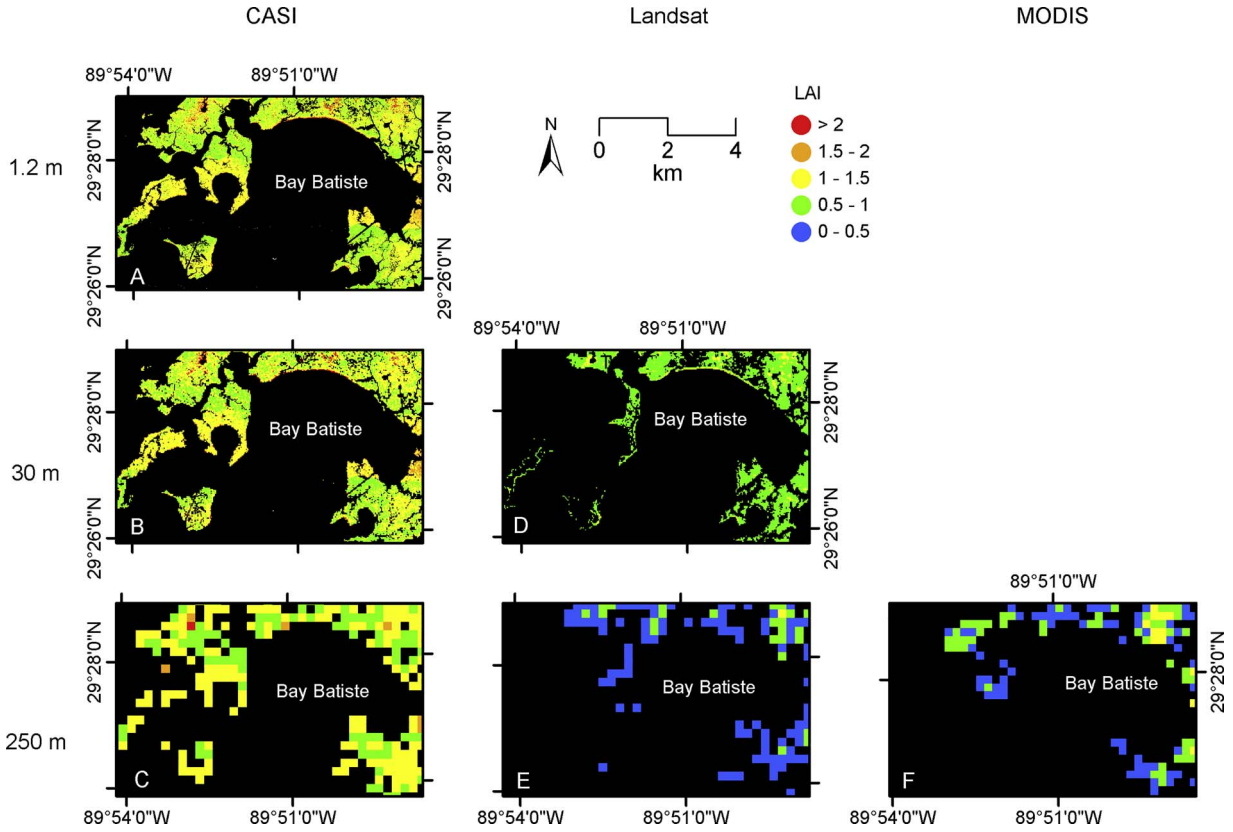

Fig. 6. Leaf area index (LAI) of coastal marshes near Bay Batiste in east Barataria Bay derived from CASI hyperspectral data, Landsat OLI imagery, and MODIS13Q1 Terra Vegetation Indices products. The LAI map derided from CASI was originally in spatial resolution of 1.2 m (A), and was downscaled into spatial resolution of 30 m (B) and 250 m (C). The LAI map derided from Landsat OLI imagery was originally in spatial resolution of 30 m (D), and downscaled into 250 m (E). The LAI map derided from MODIS13Q1data was in spatial resolution of 250 m (F).

5. Conclusions

This study samples all freshwater, intermediate, brackish, and saline marshes in Louisiana, and develops models and maps the biomass of coastal marshes in Louisiana by integrating ground, air-borne and spaceborne remote sensing data. It is found that the linear models derived from NDVI and EVI are most suitable for assessing the marshes' LAI with multispectral data (R^2 = 0.7 and 0.67, respectively), and the random forest models are most useful in retrieving the marshes' LAI and AGB with hyperspectral data (R^2 = 0.91 and 0.84, respectively). Marsh types and plant species significantly impact the development of the linear models ($P < .05$ in both cases). Maps with larger pixels yield lower LAI values, because the fine water networks are not detected and mixed into the vegetation pixels. A map derived from Landsat OLI data shows that LAI of coastal mashes in Louisiana ranges from 0 to 5.0; and is highest in freshwater marshes and in marshes in the Atchafalaya Bay delta. Maps generated from CASI data show that the LAI of saline marshes near Bay Batiste in east Barataria Bay mostly ranges from 0.9 to 1.5, and the AGB is mostly below 900 g/m^2. The results offer solutions for measuring coastal marsh biomass using various optical remote sensing techniques, and underline the influences of marsh species on model development and the sensors' spatial resolution on biomass mapping, thereby providing useful tools for assessing and monitoring the biomass of coastal marshes in Louisiana and diverse coastal marsh ecosystems elsewhere.

Acknowledgements

This research was made possible in large part by a grant from BP/Gulf of Mexico Research Initiative (GoMRI), and with financial support from the Society of Wetland Scientists (SWS). Data are publicly available through the Gulf of Mexico Research Initiative Information & Data Cooperative (GRIIDC) at https://data.gulfresearchinitiative.org (doi: 10.7266/N7ZG6Q8G, 10.7266/N7MK6BDN, 10.7266/N7GT5KPX, 10.7266/N7C24TX2). The authors are thankful to the Louisiana Universities Marine Consortium (LUMCON) and the National Center for Airborne Laser Mapping (NCALM), University of Houston, for field and laboratory support.

Appendix

Table A1
Designations of the blue, red, and near infrared bands in the widely adopted multispectral satellite sensors for calculating broad-band vegetation indices: Advanced Spaceborne Thermal Emission and Reflection Radiometer (ASTER), Advanced Very High Resolution Radiometer (AVHRR), the Landsat Multispectral Scanner(MSS), Landsat Thematic Mapper (TM), Landsat Enhanced Thematic Mapper Plus (ETM +), Landsat Operational Land Imager (OLI), Moderate Resolution Imaging Spectroradiometer (MODIS), Satellite Pour l'Observation de la Terre (SPOT), and SENTINEL-2 MultiSpectral Instrument (MSI). (http://landsat.usgs.gov/band_designations_landsat_satellites.php; https://www.ngdc.noaa.gov/ecosys/cdroms/AVHRR97_d1/avhrr.htm; http://modis.gsfc.nasa.gov/about/specifications.php; http://www.geo-airbusds.com/en/194-resolution-and-spectral-bands; https://earth.esa.int/web/sentinel/user-guides/sentinel-2-msi/resolutions/radiometric).

Satellite/Sensor	Blue Band		Red Band		Near Infrared Band		Spatial Resolution	Temporal Span
	Band Position	Wavelength (nm)	Band Position	Wavelength (nm)	Band Position	Wavelength (nm)		
ASTER	–	–	Band 2	630–690	Band 3	760–860	15 m	1999–present
AVHRR/3	–	–	Band 1	580–680	Band 2	725–1000	1.1 km	1978–present
Landsat MSS	–	–	Band 5	600–700	Band 6	700–800	60 m	1972–2013
Landsat TM	Band 1	450–520	Band 3	630–690	Band 4	760–900	30 m	1982–2013
Landsat ETM+	Band 1	450–520	Band 3	630–690	Band 4	770–900	30 m	1999–present
Landsat OLI	Band 2	450–510	Band 4	640–670	Band 5	850–880	30 m	2013–present
MODIS	Band 3	459–479	Band 1	620–670	Band 2	841–876	250 m (Band 1–2) 500 m (Band 3)	1999–present
Sentinel-2 MSI	Band 2	458–522	Band 4	650–680	Band 8	785–899	10 m	2015–present
SPOT	–	–	Band 2	610–680	Band 3	780–890	10 or 20 m	1986–present

Table A2
Vegetation indices used to develop linear models: Simple ratio (SR), normalized vegetation index (NDVI), Atmospherically Resistant Vegetation Index (ARVI), Soil-Adjusted Vegetation Index (SAVI), Soil and Atmospherically Resistant Vegetation Index (SARVI), and Enhance Vegetation Indices (EVI).

Equation	Note	Source
$SR = \frac{R}{NIR}$	SR is the earliest developed vegetation indices especially sensitive for high biomass vegetation.	Birth and McVey (1968), Jordan (1969)
$NDVI = \frac{NIR - R}{NIR + R}$	NDVI reduces sources of noise present in multiply bands such as illumination differences and atmospheric attenuation by the densitometry of red and NIR bands.	Ashley and Rea (1975)
$\frac{NIR - R}{NIR + R + L}(1 + L), L = 0.5$	SAVI uses a canopy background adjustment factor, L, to minimize soil brightness variations and eliminate the need for additional calibration for different soil.	Huete (1988)
$\frac{NIR - rb}{NIR + rb}$ $rb = R - \gamma(B - R)$, $\gamma = 1$	ARVI reduces atmospheric effects by normalizing the radiance in the blue (B), red, and NIR bands.	Kaufman and Tanre (1992)
$\frac{NIR - rb}{NIR + rb + L}(1 + L)$ $rb = R - \gamma(B - R)$, $\gamma = 1$	SARVI integrates the usage of the L function in SAVI and the blue reflectance in ARVI to correct for both soil and atmospheric noises.	Huete and Liu (1994)
EVI = , $G \times \frac{NIR - R}{NIR + C_1 \times R - C_2 \times B + C_3}$, G (gain factor) = 2.5, $C_1 = 6, C_2 = 7.5, C_3 = 1$	EVI uses the blue reflectance with two coefficients, C_1 and C_2, to correct atmospheric aerosol scattering in the red reflectance, and a soil adjustment factor, C_3, to decouple the background signal.	Huete et al. (2002)

Table A3
Collection time of the Landsat datasets.

Scenes		Collected Time	
Path	Row	Date	Julian Day
24	39	2015 Sep 17	260
24	40	2015 Sep 17	260
23	39	2015 Aug 25	237
23	40	2015 Aug 25	237
22	39	2015 Aug 2	214
22	40	2015 Aug 2	214
21	39	2015 Aug 27	239
21	40	2015 Jul 26	207

Table A4
Linear models derived from the simulated CASI data (band 380–855 nm) for predicting the marshes leaf area index (LAI) and aboveground green biomass (AGB).

Variables/ bands	Model for LAI (R^2 = 0.93)		Model for AGB (R^2 = 0.71)	
	Coefficients	Standard Error	Coefficients	Standard Error
Intercept	−1.082e-02	3.532e-01	691.4	298.2
370	–	–	−467838.5	123463.8
385	−8.368e+02	2.133e+02	–	–
400	1.086e+03	3.894e+02	866363.9	216315.1
414	−1.139e+03	5.645e+02	−584770.0	249753.8
428	2.696e+03	9.378e+02	−493031.4	470443.6
442	−2.754e+03	1.170e+03	2107711.6	690142.9
456	2.265e+03	1.071e+03	−2871936.3	767364.3
471	−3.326e+03	1.089e+03	1221765.6	490885.8
485	4.632e+03	1.439e+03	–	–
499	−5.261e+03	1.804e+03	–	–
513	4.016e+03	9.717e+02	738703.9	368588.6
528	−1.648e+03	7.458e+02	−984505.0	618756.3
542	−8.849e+02	7.064e+02	1134057.8	532079.1
556	1.043e+03	4.014e+02	−1279790.0	395816.2
570	5.162e+02	3.599e+02	1424057.5	411408.7
585	–	–	−1696468.0	643832.8
599	−3.141e+02	3.613e+02	697249.3	332722.5
613	−3.732e+02	2.349e+02	350464.3	105728.8
627	−4.837e+02	3.972e+02	–	–
642	3.547e+02	3.157e+02	456739.6	168861.0
656	1.223e+03	3.661e+02	−1319669.6	244426.6
670	−1.018e+03	3.155e+02	1150653.7	292058.1
684	2.770e+02	2.096e+02	−672129.1	223271.5
699	−1.633e+02	9.145e+01	212912.9	177406.0
713	–	–	−182225.4	154400.8
727	–	–	340031.0	180454.1
741	1.360e+02	4.276e+01	−436661.0	203830.9
756	−1.630e+02	7.358e+01	291289.8	115436.4
784	3.480e+02	1.658e+02	228378.5	84675.9
798	−5.450e+02	1.566e+02	−695302.2	169242.3
798	–	–	585854.0	119172.1
813	2.603e+02	5.407e+01	–	–
827	–	–	−234599.7	92059.1
841	–	–	−148582.0	115979.6
855	–	–	200690.4	75659.4

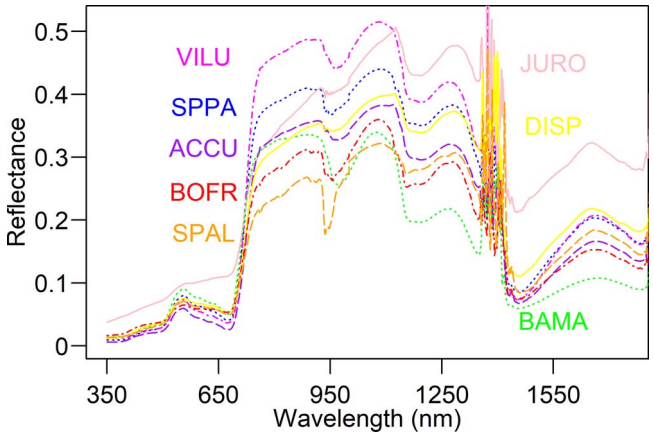

Fig. A1. Spectra of several dominant species in the study area: *Vigna luteola* (magenta), *Juncus roemerianus* (pink), *Spartina patens* (blue), *Distichlis spicata* (yellow), *Acnida cuspidate* (purple), *Borrichia frutescens* (red), *Spartina alterniflora* (orange), and *Batis maritima* (green). (For interpretation of the references to colour in this figure legend, the reader is referred to the web version of this article.)

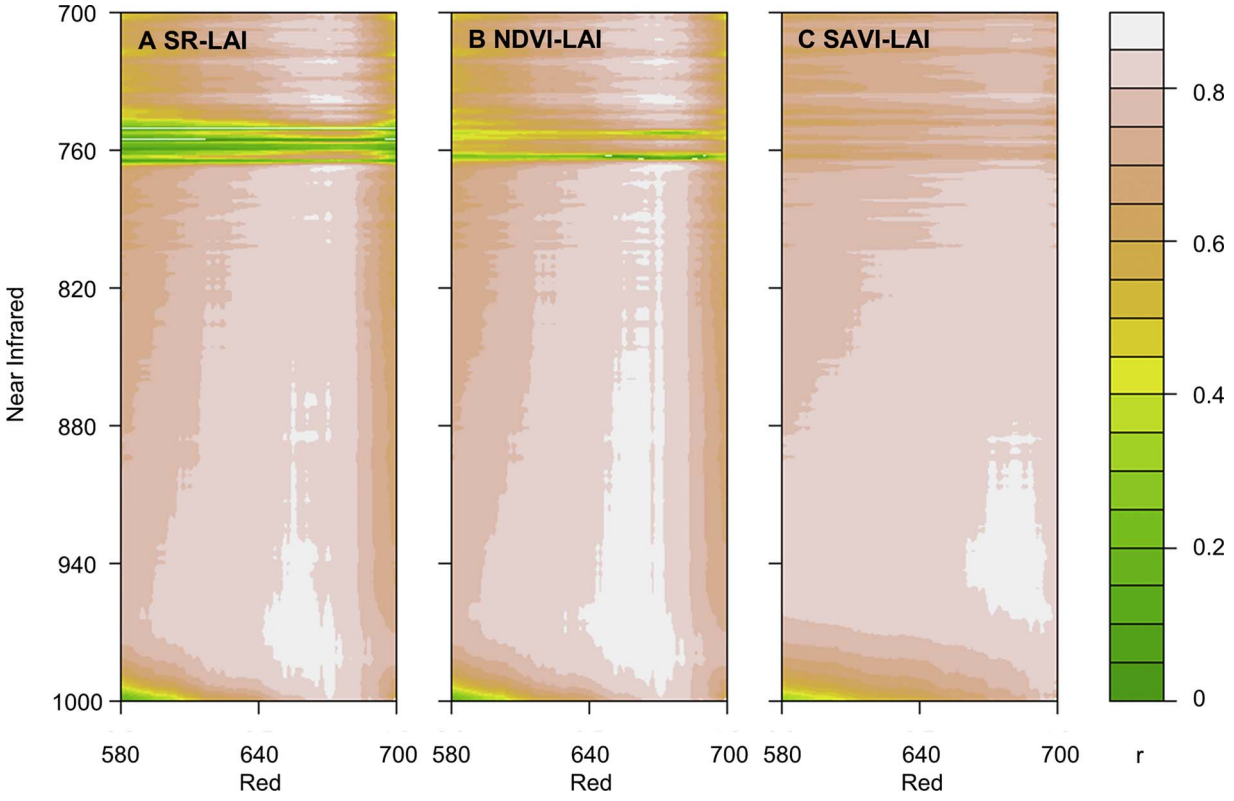

Fig. A2. Correlation coefficients (r) between LAI and the narrowband (A) SR, (B) NDVI, and (C) SAVI calculated from all possible band combinations from red and NIR wavelengths. (For interpretation of the references to colour in this figure legend, the reader is referred to the web version of this article.)

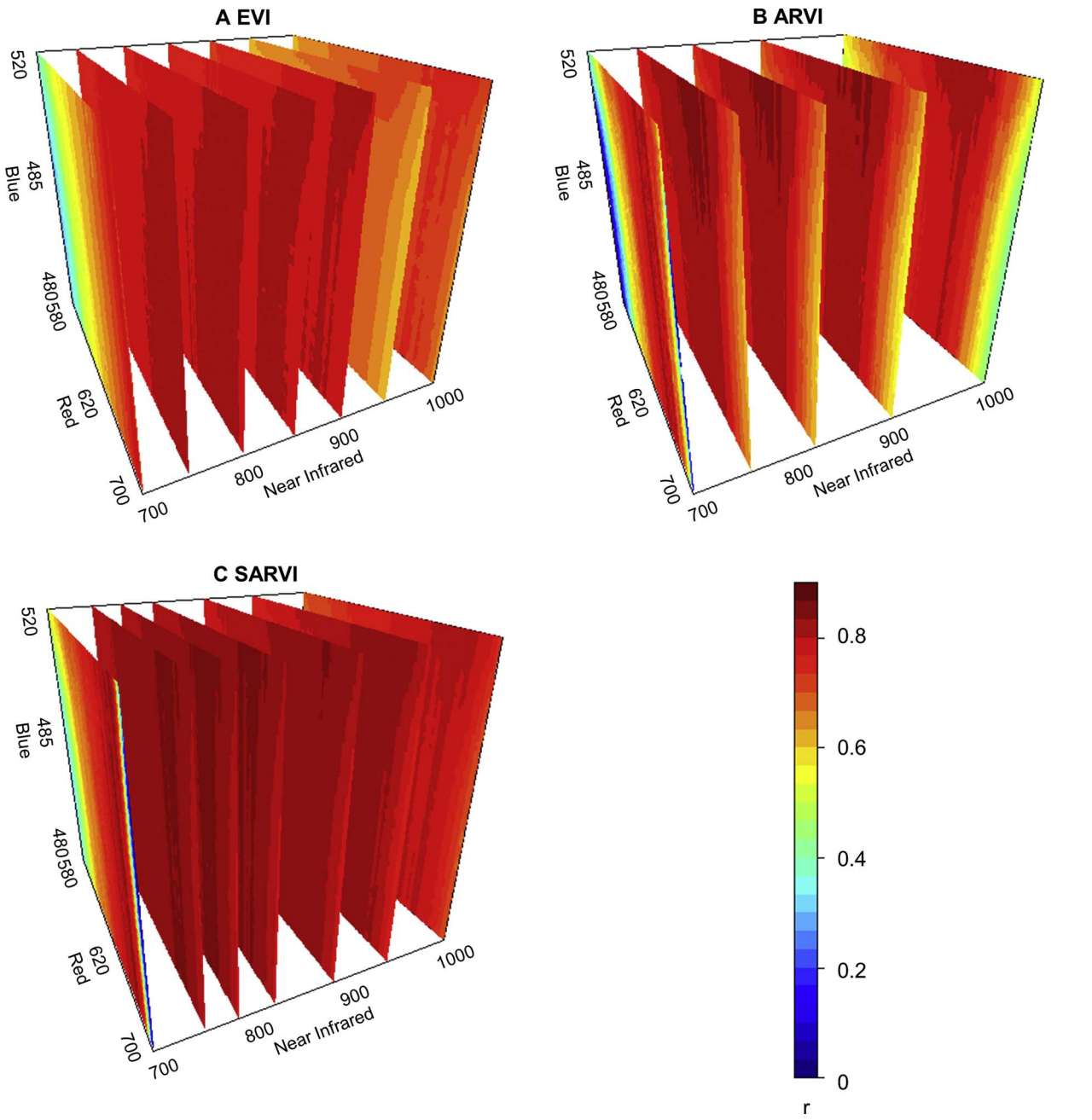

Fig. A3. Correlation coefficients (r) between LAI and the narrowband (A) EVI, (B) ARVI, and (C) SARVI calculated from all possible band combinations from the blue, red, and NIR wavelengths. (For interpretation of the references to colour in this figure legend, the reader is referred to the web version of this article.)

References

Ashley, M.D., Rea, J., 1975. Seasonal vegetation differences from ERTS imagery. Photogramm. Eng. Remote Sens. 41, 713–719.

Asrar, G., Kanemasu, E.T., Yoshida, M., 1985. Estimates of leaf area index from spectral reflectance of wheat under different cultural practices and solar angle. Remote Sens. Environ. 17, 1–11.

Birth, G.S., McVey, G.R., 1968. Measuring color of growing turf with a reflectance spectrophotometer. Agron. J. 60, 640–643.

Byrd, K.B., O'Connell, J.L., Di Tommaso, S., Kelly, M., 2014. Evaluation of sensor types and environmental controls on mapping biomass of coastal marsh emergent vegetation. Remote Sens. Environ. 149, 166–180.

Chabreck, R.H., 1972. Vegetation, Water and Soil Characteristics of the Louisiana Coastal Region. Louisiana State University and Agricultural and Mechanical College, Agricultural Experiment Station, Baton Rouge, LA.

Cutler, D.R., Edwards, T.C., Beard, K.H., Cutler, A., Hess, K.T., 2007. Random forests for classification in ecology. Ecology 88, 2783–2792.

Deegan, L.A., Johnson, D.S., Warren, R.S., Peterson, B.J., Fleeger, J.W., Fagherazzi, S., Wollheim, W.M., 2012. Coastal eutrophication as a driver of salt marsh loss. Nature 490, 388–392.

Ghosh, S., Mishra, D.R., Gitelson, A.A., 2016. Long-term monitoring of biophysical characteristics of tidal wetlands in the northern Gulf of Mexico – A methodological approach using MODIS. Remote Sens. Environ. 173, 39–58.

Good, R.E., Whigham, D.F., Simpson, R.L., 1978. Freshwater Wetlands: Ecological Processes and Management Potential. Academic Press, New York.

Gosselink, J.G., 1984. The Ecology of Delta Marshes of Coastal Louisiana: a Community Profile. U. S. Fish and Wildlife Service.

Gross, M.F., Klemas, V., Levasseur, J.E., 1986. Remote sensing of *Spartina anglica* biomass in five french salt marshes. Int. J. Remote Sens. 7, 657–664.

Gross, M.F., Hardisky, M.A., Klemas, V., Wolf, P.L., 1987. Quantification of biomass of the marsh grass *Spartina alterniflora* Loisel using Landsat thematic mapper imagery. Photogramm. Eng. Remote Sens. 53, 1577–1583.

Gross, M.F., Hardisky, M.A., Wolf, P.L., Klemas, V., 1993. Relationships among *Typha* biomass, pore water methane, and reflectance in a Delaware (U.S.A.) brackish marsh. J. Coast. Res. 9, 339–355.

Hardisky, M.A., Smart, R.M., Klemas, V., 1983. Growth response and spectral characteristics of a short *Spartina alterniflora* saltmarsh irrigated with freshwater and sewage effluent. Remote Sens. Environ. 13, 57–67.

Hopkinson, C.S., Gosselink, J.G., Parrondo, R.T., 1978. Aboveground production of seven marsh plant species in coastal Louisiana. Ecology 59, 760–769.

Howes, N.C., FitzGerald, D.M., Hughes, Z.J., Georgiou, I.Y., Kulp, M.A., Miner, M.D., Smith, J.M., Barras, J.A., Thomas, D.H., 2010. Hurricane-induced failure of low salinity wetlands. Proc. Natl. Acad. Sci. U. S. A. 107, 14014–14019.
Huete, A.R., Liu, H.Q., 1994. An error and sensitifity analysis of teh atmosperic- and soil-correcting variants of the NDVI for the MODIS-EOS. IEEE Trans. Geosci. Remote Sens. 32, 897–905.
Huete, A., Didan, K., Miura, T., Rodriguez, E.P., Gao, X., Ferreira, L.G., 2002. Overview of the radiometric and biophysical performance of the MODIS vegetation indices. Remote Sens. Environ. 83, 195–213.
Huete, A.R., 1988. A soil-adjusted vegetation index (SAVI). Remote Sens. Environ. 25, 295–309.
Jensen, J.R., Coombs, C., Porter, D., Jones, B., Schill, S., White, D., 1998. Extraction of smooth cordgrass (*Spartina alterniflora*) biomass and leaf area index parameters from high resolution imagery. Geocarto Int. 13, 25–34.
Jensen, J.R., Olson, G., Schill, S.R., Porter, D.E., Morris, J., 2002. Remote sensing of biomass, leaf-area-index, and chlorophyll a and b content in the ACE basin national Estuarine research reserve using sub-meter digital camera imagery. Geocarto Int. 17, 27–36.
Jordan, C.F., 1969. Derivation of leaf area index from quality of light on forest floor. Ecology 50, 663–666.
Kaufman, Y.J., Tanre, D., 1992. Atmospherically resistant vegetation index (ARVI) for EOS-MODIS. IEEE Trans. Geosci. Remote Sens. 30, 261–270.
Kearney, M.S., Stutzer, D., Turpie, K., Stevenson, J.C., 2009. The effects of tidal inundation on the reflectance characteristics of coastal marsh vegetation. J. Coast. Res. 25, 1177–1186.
Kulawardhana, R.W., Popescu, S.C., Feagin, R.A., 2014. Fusion of lidar and multispectral data to quantify salt marsh carbon stocks. Remote Sens. Environ. 154, 345–357.
Liaw, A., Wiener, M., 2002. Classification and Regression by randomForest. R news 2, pp. 18–22.
Liu, J.G., Pattey, E., 2010. Retrieval of leaf area index from top-of-canopy digital photography over agricultural crops. Agric. For. Meteorol. 150, 1485–1490.
Morris, J.T., Sundareshwar, P.V., Nietch, C.T., Kjerfve, B., Cahoon, D.R., 2002. Responses of coastal wetlands to rising sea level. Ecology 83, 2869–2877.
Penfound, W.T., Hathaway, E.S., 1938. Plant communities in the Marshlands of Southeastern Louisiana. Ecol. Monogr. 8, 4–56.
Trilla, G.G., Pratolongo, P., Beget, M.E., Kandus, P., Marcovecchio, J., Di Bella, C., 2013. Relating biophysical parameters of coastal marshes to hyperspectral reflectance data in the Bahia Blanca Estuary, Argentina. J. Coast. Res. 29, 231–238.
Visser, J., Sasser, C., Chabreck, R., Linscombe, R.G., 1998. Marsh vegetation types of the Mississippi River deltaic plain. Estuaries 21, 818–828.
Visser, J.M., Sasser, C.E., Cade, B.S., 2006. The effect of multiple stressors on salt marsh end-of-season biomass. Estuar. Coast. 29, 328–339.
Visser, J.M., Day, J.W., Battaglia, L.L., Shaffer, G.P., Hester, M.W., 2012. Mississippi River Delta Wetlands. pp. 63–74.
Waide, R.B., Willig, M.R., Steiner, C.F., Mittelbach, G., Gough, L., Dodson, S.I., Juday, G.P., Parmenter, R., 1999. The relationship between productivity and species richness. Annu. Rev. Ecol. Evol. Syst. 30, 257–300.
Zhang, M., Ustin, S.L., Rejmankova, E., Sanderson, E.W., 1997. Monitoring Pacific coast salt marshes using remote sensing. Ecol. Appl. 7, 1039–1053.
Zhao, D.H., Xie, D., Zhou, H.J., Jiang, H., An, S.Q., 2012. Estimation of leaf area index and plant area index of a submerged macrophyte canopy using digital photography. PLoS One 7.